Electronic Supporting Material
for
Enhanced detection of acetamiprid via a gold nanoparticle-based colorimetric aptasensor integrated with hybridization chain reaction

Xingyi Liu,[a] Mingming Li,[a] Hao Wang,[a] and Limin Yang,[a,*]

[a]Center for Bioengineering and Biotechnology, College of Chemistry and Chemical Engineering, China University of Petroleum (East China), Qingdao 266580, P. R. China
*Correspondence: yanglimin@upc.edu.cn (Limin Yang)

This material includes:

1. Oligonucleotide sequences

Table S1 Oligonucleotide sequences used in the experiments.[a]

Items	Sequence（5′ to 3′）
cDNA	SH-TTTTTTTTTCTTCATAATATGGTGTCAG
ABA	TTTGTCTGCAGCGGTTCTTGATCGCTGACACCATATTATGAAGA
H1	*CGATCA***AGAACCGCTGCAGACAAA**CGGCAT**TTTGTCTGCAGCGGTTCT**
H2	**TTTGTCTGCAGCGGTTCT**TGATCG**AGAACCGCTGCAGACAAA***ATGCCG*
P	TCAATTGACACTCAGACCCGGTACTCAACTATTCCCTCACATAA
P’	SH-TTTTTTTTTTATGTGAGGGAATAGTTGA

[a]The underlined sequence in the ABA chain is the initiator for the HCR. In the hairpins, boldface type indicates stem sequences and italic type shows toehold ends.

2. Characterization of CQDs

The carbon quantum dots (CQDs) were meticulously characterized using UV-visible absorption spectroscopy, fluorescence spectroscopy, transmission electron microscopy (TEM), and Fourier-transform infrared (FTIR) spectroscopy. **Figure S1A** showcases the distinct absorption and fluorescence emission patterns exhibited by the CQDs. Notably, the use of amino-functionalized polyethylene glycol-treated CQDs resulted in a prominent absorption peak at 480 nm. For the experimental configuration, a 470 nm excitation wavelength was chosen, leading to an emission peak position of 523 nm for the CQDs.

To delve deeper into the morphology of the CQDs, TEM analysis was conducted, and the outcomes are presented in **Figure S1B**. The CQDs exhibited a distinctly spherical structure with a dispersed distribution. A high-resolution TEM image further revealed that the lattice spacing of the CQD measured 0.27 nm, attributed to the (100) plane of the graphitic core or aromatic carbon.[1]

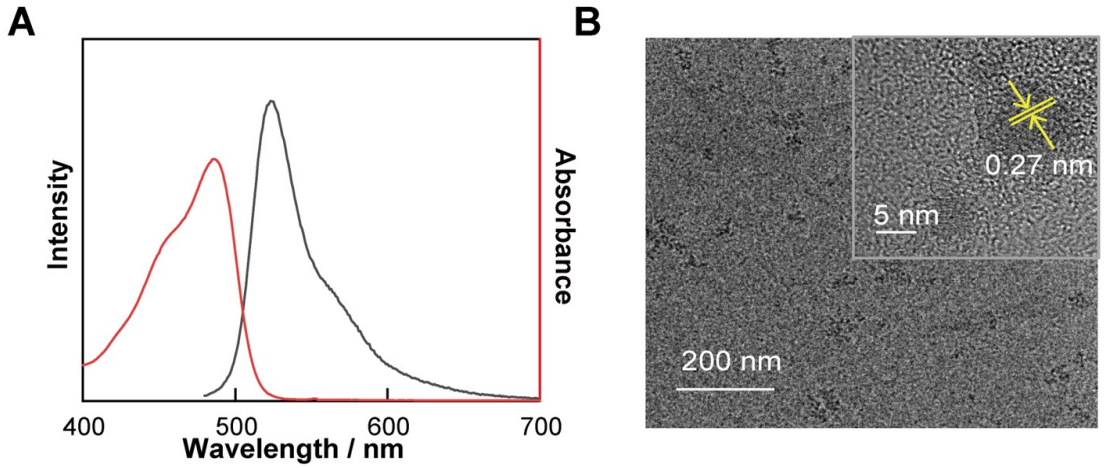

Figure S1 (A) Absorption and fluorescence spectra of CQDs. (B) TEM image of CQDs. The upper right corner displays a high-resolution TEM image.

The FTIR spectra presented in **Figure S2** offer profound insights into the chemical composition and bonding patterns of CQDs. Notably, distinct peaks were observed at 3443 cm^{-1} and 2914 cm^{-1}, indicative of the stretching vibrations of N-H and C-H bonds, respectively.[2] Additionally, the absorption peak at 1631 cm^{-1} is associated with the C=O stretching vibration,[3] whereas the peak at 1466 cm^{-1} corresponds to the absorption peaks of –COO–[4]. These observations suggest the presence of -COOH groups on the CQDs surface, enhancing their hydrophilicity and stability in aqueous

solutions. Furthermore, the absorption band at 1356 cm^{-1} reflects the C-NH bending vibration. A minor absorption peak at 1102 cm^{-1} is attributed to the C-O stretching vibration,[5] and the peak near 783 cm^{-1} corresponds to the -CH_2 bending vibration. Collectively, these peaks confirm the infrared spectral characteristics typical of CQDs.

Figure S2 FTIR spectrum of CQDs.

3. Preparation and characterization of AuNPs

The AuNPs were synthesized by the sodium citrate method. Briefly, 100 mL of 1 mM $HAuCl_4$ solution was heated to boiling under constant stirring. Rapidly, 10 mL of 38.8 mM citrate solution was added. After waiting for 6 min, the solution color will undergo a significant change, transforming from a light yellow to a wine red. Subsequently, heating is continued for an additional 10 min before being terminated. The solution is then allowed to cool down to room temperature. The AuNP colloidal solution was prepared.

The AuNPs as prepared were characterized by UV-vis spectroscopy and TEM. UV-vis spectrophotometric analysis revealed a prominent absorption peak centered at approximately 520 nm (**Figure S3A**), corresponding to the surface plasmon resonance band of AuNPs. The narrowness of the absorption peak indicates the uniformity and excellent monodispersity of the particles synthesized using this method. TEM image (**Figure S3B**) further confirmed these observations, revealing uniformly spherical particles. Additionally, the average particle size was determined to be 13 nm. Elemental mapping result (**Figure S3C**) reveals a substantial presence of Au elements in the nanoparticles, thereby corroborating their identity as AuNPs. According to published literature,[6] the extinction coefficient for 12 nm AuNPs is 2.01×10^8 M^{-1} cm^{-1}. By applying Lambert-Beer's law, we calculated the concentration of AuNPs to be 11 nM.

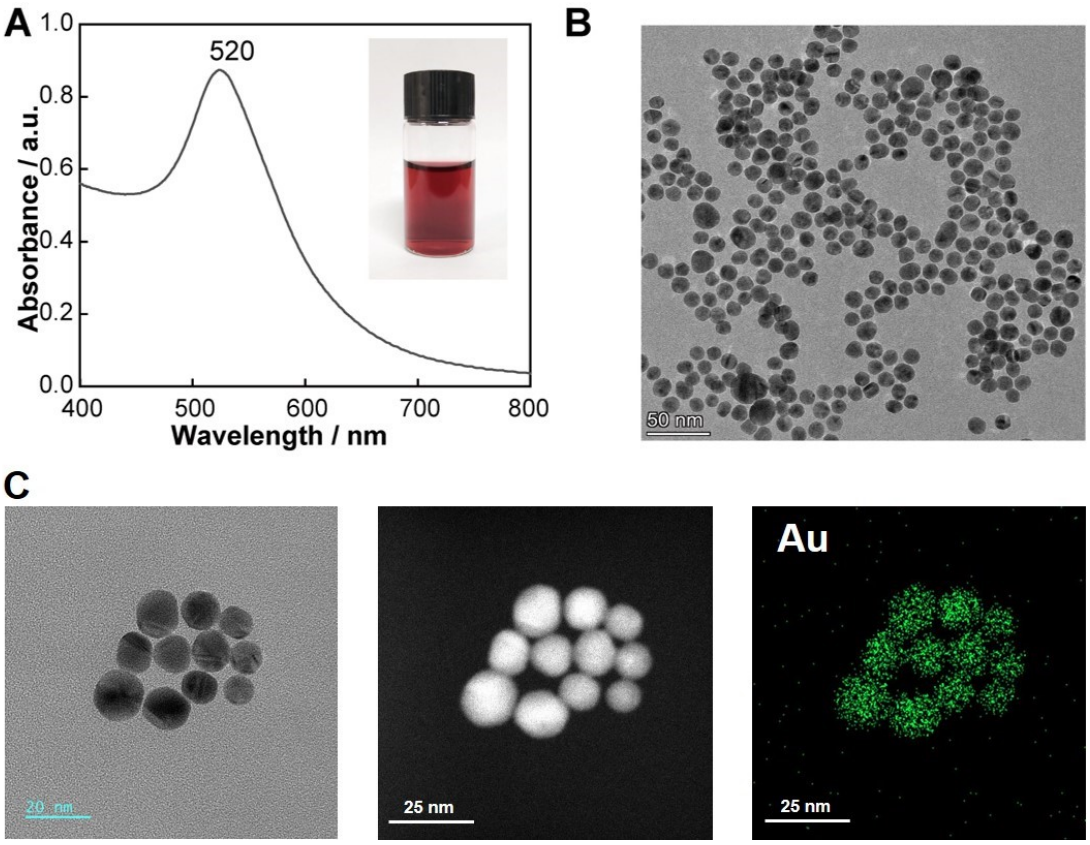

Figure S3 Characterization of AuNPs.

4. NUPACK simulation of hairpins

The secondary structures of the H1 and H2 sequences were simulated using the NUPACK software, as shown in **Figure S4A** and **S4B**, respectively. The simulation results validate the formation of the expected hairpin structure and ensure the structural integrity and stability of these sequences in subsequent HCR.

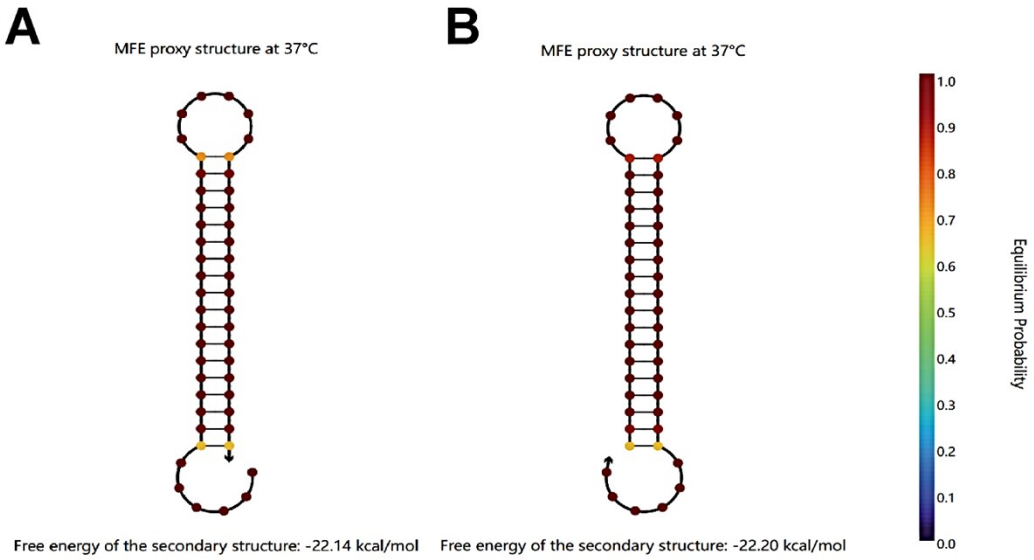

Figure S4 NUPACK simulation of (A) H1 and (B) H2 sequences.

5. TEM characterization of dsDNA-AuNPs after interacting with acetamiprid and HCR-AuNPs

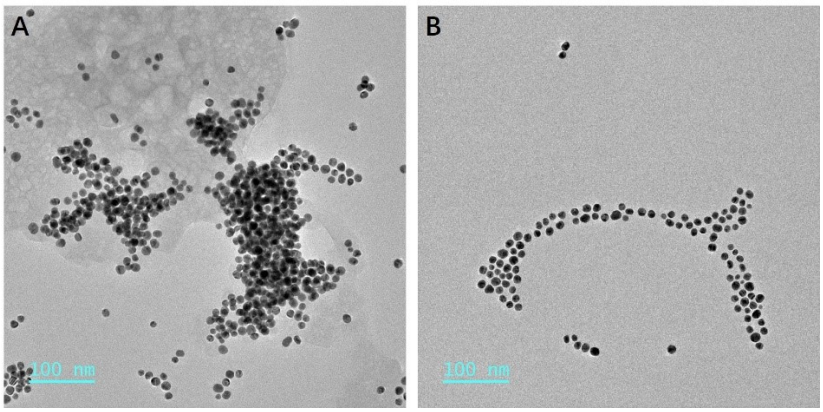

Figure S5 TEM characterization results for (A) dsDNA-AuNP at a concentration of 0.04 M NaCl after interacting with acetamiprid, and (B) HCR-AuNPs at the same NaCl concentration.

6. Aggregation behavior of P-P'-AuNPs

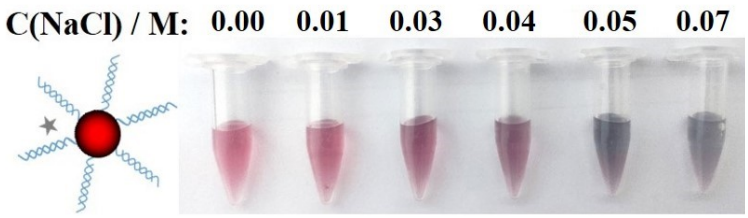

Figure S6 Aggregation behavior of P-P'-AuNPs.

7. Results of the optimization experiments

Initially, we assessed the detection efficiency of dsDNA-AuNP probes prepared with varying ABA concentrations ranging from 20 to 120 μM. As depicted in **Figure S7A**, it is evident that while the response signal diminishes gradually with increasing ABA concentration, this trend suggests that a higher loading of ABA on the AuNPs' surface favors enhanced interaction with acetamiprid, thus boosting sensitivity. Nevertheless, the overall change in signal magnitude was modest, particularly for ABA concentrations exceeding 60 μM. Considering both sensitivity and cost, we determined 100 μM as the optimal ABA concentration for our experiments. Subsequently, we analyzed the effect of the probe's interaction time with acetamiprid on detection performance. As shown in **Figure S7B**, when the reaction time was less than 5 min, a high A_{520}/A_{650} signal was recorded. This indicates that the binding process between the probe and the target requires a specific duration to reach completion. A shorter reaction time may lead to incomplete binding, resulting in reduced detection sensitivity and a weaker signal. As the reaction time increased, we observed a gradual enhancement in the binding efficiency between the probe and the target, reflected in a lower A_{520}/A_{650} ratio. However, further extending the reaction time beyond 10 min yielded minimal changes in the signal. Therefore, we selected a 10-minute reaction time as the optimal duration for our experimental setup.

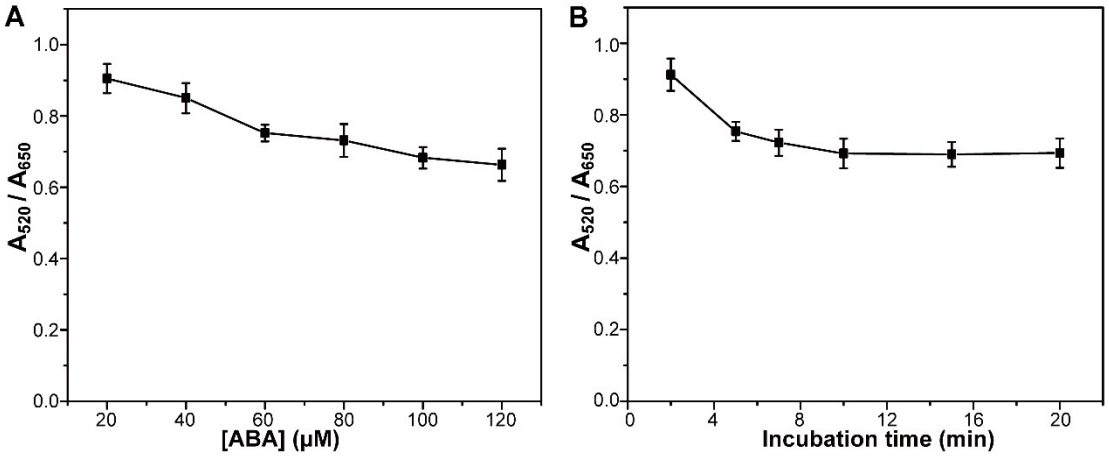

Figure S7 The response of the dsDNA-AuNP probes on 0.08 μM acetamiprid under different (A) ABA concentrations and (B) incubation times.

8. Comparison of the performance of AuNP-based colorimetric aptasensing methods for the detection of acetamiprid

Table S2 Comparison of the performance of AuNP-based colorimetric aptasensing methods for the detection of acetamiprid.

Methods	Attachment	Mechanism	Linear range	Detection limit	Ref.
A colorimetric detection method based on an unlabeled aptamer and AuNPs	Adsorption	Aggregation of AuNPs	1.5 ~ 60 μM	0.0559 μM	[7]
Colorimetric detection with HCR-assisted amplification and smartphone readout strategy	Adsorption	Aggregation of AuNPs	0 ~ 140 μM	1.74 μM	[8]
A gold nanoparticle-based visual aptasensor using a smartphone	Adsorption	Aggregation of AuNPs	25 ~ 300 μM	3.81 μM	[9]
A colorimetric aptasensing with positively charged AuNPs as signal probes	Adsorption	Aggregation of AuNPs	8.7 nM ~ 0.92 μM	0.56 nM	[10]
A colorimetric aptasensing based on the enhanced peroxidase-like activity of AuNPs	Adsorption	Peroxidase activity of AuNPs	10 ~ 50 μg L^{-1} (45 ~ 225 nM)	1.02 μg L^{-1} (4.59 nM)	[11]
An AuNP-based colorimetric aptasensor integrated with HCR	Covalent bond	Aggregation of AuNPs	0.005 ~ 0.18 μM	3.14 nM	This work

References

1. Saikia, M., T. Das, and B.K. Saikia. A novel rapid synthesis of highly stable silver nanoparticle/carbon quantum dot nanocomposites derived from low-grade coal feedstock. *New Journal of Chemistry* **2021**. 46(1): 309-321.
2. Wang, J., et al. A novel fluorescent aptasensor for ultrasensitive and selective detection of acetamiprid pesticide based on the inner filter effect between gold nanoparticles and carbon dots. *Analyst* **2018**. 143(21): 5151-5160.
3. Yuan, L., et al. A novel ratiometric fluorescent probe for detection of l-glutamic acid based on dual-emission carbon dots. *Talanta* **2022**. 245: 123416.
4. Zhao, C., et al. Bi/BiOI/carbon quantum dots nano-sheets with superior photocatalysis. *Rsc Advances* **2023**. 13(43): 30520-30527.
5. Aladesuyi, O.A. and O.S. Oluwafemi. Synthesis of N, S co-doped carbon quantum dots (N,S-CQDs) for sensitive and selective determination of mercury (Hg2+) in Oreochromis niloctus (Tilapia fish). *Inorganic Chemistry Communications* **2023**. 153: 110843.
6. Maye, M.M., et al. Gold and alloy nanoparticles in solution and thin film assembly: spectrophotometric determination of molar absorptivity. *Analytica Chimica Acta* **2003**. 496(1): 17-27.
7. Tian, L., et al. A combined UV-visible with fluorescence detection method based on an unlabeled aptamer and AuNPs for the sensitive detection of acetamiprid. *New J. Chem.* **2023**. 47(16): 7722-7732.
8. Xu, C., et al. Colorimetric aptasensor for on-site detection of acetamiprid with hybridization chain reaction-assisted amplification and smartphone readout strategy. *Food Control* **2022**. 137: 108934.
9. Xu, C., et al. A gold nanoparticle-based visual aptasensor for rapid detection of acetamiprid residues in agricultural products using a smartphone. *RSC Advances* **2022**. 12(9): 5540-5545.
10. Qi, Y.Y., et al. An aptamer-based colorimetric sensing of acetamiprid in environmental samples: Convenience, sensitivity and practicability. *Sens. Actuators B: Chem.* **2020**. 304: 127359.
11. Yang, W., et al. Ultrasensitive and selective colorimetric detection of acetamiprid pesticide based on the enhanced peroxidase-like activity of gold nanoparticles. *Anal Methods* **2017**. 9(37): 5484-5493.